Uncertainty in Model Climate Sensitivity Traced to Representations of Cumulus Precipitation Microphysics

MING ZHAO

NOAA/Geophysical Fluid Dynamics Laboratory, Princeton, New Jersey, and University Corporation for Atmospheric Research, Boulder, Colorado

J.-C. GOLAZ, I. M. HELD, V. RAMASWAMY, S.-J. LIN, Y. MING, P. GINOUX, B. WYMAN, L. J. DONNER, AND D. PAYNTER

NOAA/Geophysical Fluid Dynamics Laboratory, Princeton, New Jersey

H. GUO

NOAA/Geophysical Fluid Dynamics Laboratory, Princeton, New Jersey, and University Corporation for Atmospheric Research, Boulder, Colorado

(Manuscript received 10 March 2015, in final form 26 August 2015)

ABSTRACT

Uncertainty in equilibrium climate sensitivity impedes accurate climate projections. While the intermodel spread is known to arise primarily from differences in cloud feedback, the exact processes responsible for the spread remain unclear. To help identify some key sources of uncertainty, the authors use a developmental version of the next-generation Geophysical Fluid Dynamics Laboratory global climate model (GCM) to construct a tightly controlled set of GCMs where only the formulation of convective precipitation is changed. The different models provide simulation of present-day climatology of comparable quality compared to the model ensemble from phase 5 of CMIP (CMIP5). The authors demonstrate that model estimates of climate sensitivity can be strongly affected by the manner through which cumulus cloud condensate is converted into precipitation in a model's convection parameterization, processes that are only crudely accounted for in GCMs. In particular, two commonly used methods for converting cumulus condensate into precipitation can lead to drastically different climate sensitivity, as estimated here with an atmosphere–land model by increasing sea surface temperatures uniformly and examining the response in the top-of-atmosphere energy balance. The effect can be quantified through a bulk convective detrainment efficiency, which measures the ability of cumulus convection to generate condensate per unit precipitation. The model differences, dominated by shortwave feedbacks, come from broad regimes ranging from large-scale ascent to subsidence regions. Given current uncertainties in representing convective precipitation microphysics and the current inability to find a clear observational constraint that favors one version of the authors' model over the others, the implications of this ability to engineer climate sensitivity need to be considered when estimating the uncertainty in climate projections.

1. Introduction

Numerical global climate models (GCMs) exhibit a wide range of equilibrium climate sensitivities and, consequently, a large spread in future warming projections (e.g., Randall et al. 2007; Flato et al. 2013). Uncertainty in cloud feedback is a leading cause of this disagreement (e.g., Cess et al. 1990; Soden et al. 2008). Despite decades of research to narrow uncertainties, there is still a need to pinpoint key processes that are responsible for model spread in cloud feedback (e.g., Betts and Harshvardhan 1987; Roeckner et al. 1987; Mitchell et al. 1989; Cess et al. 1990; Senior and Mitchell 1993; Bony et al. 2004; Bony and Dufresne 2005; Bony et al. 2006; Stephens 2005; Wyant et al. 2006; Webb et al. 2006; Soden and Held 2006; Dufresne and Bony 2008; Webb et al. 2013; Zelinka et al. 2013; Zhang et al. 2013; Sherwood et al. 2014; Bretherton et al. 2014; Webb et al. 2015; Bretherton 2015). This is partly due to a myriad of different assumptions coexisting

Corresponding author address: Dr. Ming Zhao, NOAA/Geophysical Fluid Dynamics Laboratory, Princeton University Forrestal Campus, 201 Forrestal Road, Princeton, NJ 08540-6649.
E-mail: ming.zhao@noaa.gov

DOI: 10.1175/JCLI-D-15-0191.1

© 2016 American Meteorological Society

in models, making it especially difficult to isolate the effect of individual processes. Nevertheless, several recent studies analyzing multimodel results from phase 5 of CMIP (CMIP5) (e.g., Sherwood et al. 2014) and perturbing individual models' physics parameters (e.g., Zhao 2014, hereinafter Z14) suggest that cumulus convection may be a key to understanding the uncertainty in cloud feedback and climate sensitivity in GCMs, supporting earlier suggestions (e.g., Somerville and Remer 1984; Murphy et al. 2004; Stainforth et al. 2005; Sanderson et al. 2008, 2010; Joshi et al. 2010).

Cumulus convection takes place over a large area of Earth's surface, manifesting itself through a variety of cloud morphologies from shallow fair weather cumulus and midlevel cumulus congestus to deep towers of cumulonimbus. Condensation and/or deposition and precipitation are essential to cumulus convection, and they occur on microscales but connect intimately with their macroscale (from 10 m to 10 km) turbulent environment. Precipitating shallow cumulus clouds are not uncommon, especially over tropical oceans (Nuijens et al. 2009).

Neither the micro nor macro processes of the cumulus convection are resolved, and therefore they must be approximated in a GCM. In particular, the representation of cumulus precipitation microphysics has been considered one of the crudest aspects of current GCMs (e.g., Emanuel and Zivkovic-Rothman 1999). Figure 1 shows a diagram of a mass flux convection scheme typically used in a GCM. Planetary boundary layer air parcels are lifted based on convective instability. As a parcel or plume rises, it cools and deposits vapor into condensate, maintaining buoyancy via latent heat release. The plume interacts with its surroundings through turbulent mixing, entrainment, detrainment, and condensate precipitation, which together modify its buoyancy and mass flux (e.g., Arakawa and Schubert 1974; Tiedtke 1989; Emanuel 1991; Moorthi and Suarez 1992; Bretherton et al. 2004). Figure 1 shows one plume, but many schemes in GCMs involve multiple plumes with different characteristics, especially for distinguishing between shallow and deep convection. Since cumulus precipitation is affected by so many complicated processes, including an ensemble of turbulent updrafts and downdrafts and associated microphysical transformations of hydrometers between various phases, sizes, and shapes, an accurate representation is not possible in current GCMs. Despite some recent attempts to incorporate more sophisticated convective microphysics (e.g., Song and Zhang 2011), most models choose a rather simple approach for determining the portion of cloud condensate converted to precipitation, with the rest being stored within a plume and/or detrained into the environment (e.g., Tiedtke 1989; Gregory and Rowntree 1990; Zhang and McFarlane 1995; Anderson et al. 2004; Emanuel and Zivkovic-Rothman 1999). Depending on details of the plume model, precipitation and detrainment of cloud condensate may be applied either at plume top (e.g., Anderson et al. 2004) or at every model level as a plume marches upward through the troposphere (e.g., Zhao et al. 2009).

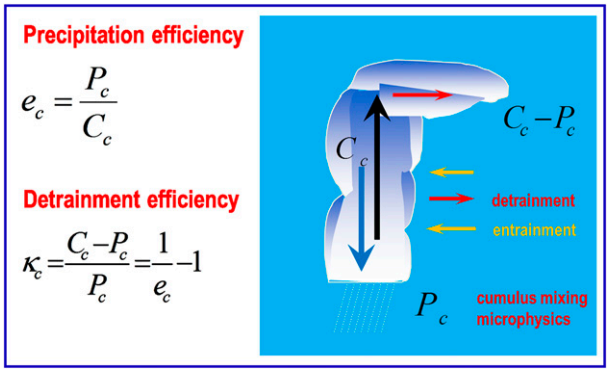

FIG. 1. A diagram for mass flux representation of convection and definitions of convective precipitation efficiency e_c and detrainment efficiency κ_c. The vertically integrated convective heating rate C_c and the surface precipitation rate P_c are both in energy units (W m^{-2}) and are globally or regionally averaged values. A bulk convective precipitation efficiency is defined by $e_c = P_c/C_c$, while $\kappa_c = (C_c - P_c)/P_c$ defines a convective detrainment efficiency (i.e., rate of cloud production by convective detrainment per unit rate of surface precipitation).

Despite many variations in implementation details, one can identify two distinct manners by which cumulus condensate is converted to precipitation. One is a threshold removal, in which all condensate exceeding a threshold value is converted to precipitation (e.g., Gregory and Rowntree 1990; Emanuel and Zivkovic-Rothman 1999; Zhao et al. 2009). The other approach is a fractional removal scheme, which assumes that a fraction of total condensate is removed as precipitation (e.g., Tiedtke 1989; Zhang and McFarlane 1995; Anderson et al. 2004). One can also consider schemes intermediate between these two extremes, in which there is a threshold before any removal occurs, with condensate above this threshold removed proportionally. Often the specifications for the fraction of precipitating condensate vary between shallow and deep convective plumes to roughly account for their differences in precipitation efficiency (e.g., Anderson et al. 2004). While threshold removal in an individual updraft may be more plausibly connected to the microphysical requirements for precipitation, the threshold values used in GCMs are often only crudely determined and may not be directly compared to observations (e.g., Suzuki et al. 2013). Moreover, it is hard to argue which scheme is more realistic when

representing the collective rate of precipitation from a cumulus ensemble, especially when mixed- or ice-phase clouds are present and when considering that the plume model itself is already a poor representation of cumulus clouds. Indeed, the fractional removal method has also been widely used in a number of GCMs, including the GFDL Atmospheric Model version 2 (AM2; Anderson et al. 2004), NCAR CAM5 (Zhang and McFarlane 1995), and MPI ECHAM6 (Stevens et al. 2013). Thus, we note that both the formulations and the parameters used in individual GCMs may apply only to model implementation and not necessarily to nature. The crude representations of convective precipitation processes may be the cause of some important GCM biases, including the too light and too frequent precipitation problem found in virtually all current GCMs (e.g., Stephens et al. 2010; Suzuki et al. 2013).

GCMs also include microphysical assumptions that control condensation on the grid scale. Our concern here is focused on the production of condensate by GCMs' convection schemes, not the resolved-scale condensation. In this study, we explore these two commonly used methods for converting cumulus condensate into precipitation in a single developmental version of an atmospheric model with differences confined entirely in the treatment of convective precipitation. Without impacting the quality of the climate simulation appreciably, we demonstrate that the two methods can lead to drastically different climate sensitivity. We further show that the effect can be understood through a bulk convective detrainment efficiency, which measures the ability of cumulus convection to generate clouds and moisten the free troposphere per unit precipitation (Z14). Figure 1 provides a definition of the convective detrainment efficiency, $\kappa_c = (C_c - P_c)/P_c$, where P_c and C_c are, respectively, globally (or regionally) averaged surface convective precipitation rate and column-integrated convective heating rate (see Z14; P_c and C_c are both in energy units). We argue that κ_c is a key for understanding cloud feedback and climate sensitivity in relation to convection parameterization. Section 2 describes the model and simulation setup. Section 3 presents the results. Section 4 provides a summary and discusses the implications of having an ability to engineer climate sensitivity in the absence of clear observational constraints on cumulus precipitation microphysical processes.

2. The model and simulation setup

The model used here is a developmental version of the GFDL new-generation Atmospheric Model, version 4 (AM4). AM4 began with an integration of two streams of existing models [AM3 (Donner et al. 2011) and HiRAM (Zhao et al. 2009)] and the creation of a new prototype model. The new model incorporates the prognostic aerosols and aerosol-cloud physics in AM3 with the higher spatial resolution used in HiRAM. To reduce computational cost, the fully interactive atmospheric chemistry in AM3 is reduced to gas and aqueous phases sulfate chemistry only, which includes three prognostic equations for SO_4, SO_2, and H_2O_2 while all other chemical species are fixed climatological (1980–2000) monthly mean based on simulations by Donner et al. (2011). While the target resolution for AM4 is 50 km, much of the development has taken place in a 100-km configuration. Based on a developmental version of the 100-km resolution AM4, we have created three models [denoted below as the high- (H), medium- (M), and low- (L) sensitivity models], which are identical in all aspects of the dynamics and physics formulations except the treatment of cumulus precipitation.

The convection scheme is based on a modified version of the University of Washington Shallow Cumulus (UWShCu) scheme (Bretherton et al. 2004) similar to that used in HiRAM (Zhao et al. 2009). In addition to the single plume used in HiRAM, we have included a second plume for representing deep convection. Appendix A provides the motivations for this development and a description of the changes made to the convection scheme. Below, we only focus on the differences between H, M, and L to explore the role of convective precipitation treatment on cloud feedback and climate sensitivity. The results and conclusions do not depend on the specific version of AM4 used. We have repeated a similar set of experiments for various developmental versions of AM4 as well as HiRAM. The sensitivity of cloud feedback to the different treatments of convective precipitation is robust across all the GFDL models we explored.

As parameterized convective plumes move upward, H follows HiRAM and the shallow convection scheme of AM3, assuming a threshold removal for precipitation P, precipitating the portion of total condensate q_c in excess of q_{c0}: that is,

$$P = M_c \max(q_c - q_{c0}, 0),$$
$$q_{c0} = \begin{cases} q_0, & T \geq 0^\circ\mathrm{C} \\ q_0\left(1 - \dfrac{T}{T_{\mathrm{crit}}}\right), & T_{\mathrm{crit}} < T < 0^\circ\mathrm{C} \\ 0, & T \leq T_{\mathrm{crit}} \end{cases}, \quad (1)$$

where M_c denotes convective mass flux. The threshold value q_{c0} is set to q_0 for warm clouds and decreases linearly with temperature T for $T < 0^\circ$C to account for ice effects (Emanuel and Zivkovic-Rothman 1999). The critical temperature is T_{crit} in degrees Celsius, below which q_{c0} is set to 0; q_0 and T_{crit} are two parameters

that can be adjusted to optimize the model's clouds and cloud radiative effect.

In contrast to H, both M and L utilize a fractional removal scheme for precipitation similar in concept to that in AM2. To account for the threshold behavior associated with the warm rain autoconversion process, as a plume rises through a model layer, we set precipitation to be

$$P = M_c \beta \delta p \max(q_c - q_{c0}, 0), \quad q_{c0} = \begin{cases} q_0, & T \geq -5^\circ\mathrm{C} \\ 0, & T < -5^\circ\mathrm{C} \end{cases}. \tag{2}$$

If q_0 is set to 0, this scheme becomes completely a fractional removal scheme for both warm and cold clouds. Here, β represents a precipitation efficiency parameter (Pa^{-1}), and δp denotes the pressure depth of a model layer so that the specification of β is independent of the model's vertical resolution ($\beta\delta p$ is capped at 1). We distinguish the precipitation efficiency β between warm/shallow and cold/deep clouds by setting $\beta = \beta_l$ when $T \geq -5^\circ$C, and $\beta = \beta_i$ when $T \leq -25^\circ$C, with β_l being smaller than β_i. The parameter β is linearly interpolated between -5° and -25°C. Since in nature the accretion process in deep convective clouds can significantly enhance precipitation efficiency, we represent it by making the pair of (β_l, β_i) in deep convective plumes proportionally larger than those used for shallow convective plumes with the proportionality constant denoted as α ($\alpha > 1$). The parameters q_0, β_l, β_i, and α are adjustable for cloud tuning in M and L. To explore the impact of α, we set $\alpha = 1$ for L so that deep and shallow convective plumes use the same set of values for β_l and β_i.

H, M, and L were individually tuned to reproduce reasonably well the observed present-day climate (both global means and spatial distributions) when forced by the observed climatological SSTs from the Met Office HadISST, version 1.1 (Rayner et al. 2003). The tuning of each model, however, does not involve any parameter changes outside its convective precipitation scheme so that the differences between H, M, and L are confined entirely in their representations of convective precipitation. In this study, parameters such as β_l, β_i, and q_0 are considered as adjustable parameters for model optimization and the tuning of the top-of-atmosphere (TOA) net radiative flux close to balance. Table 1 provides a list of the parameters used in H, M, and L and their simulated global mean quantities for TOA cloud radiative effect (CRE) and its longwave (LW) and shortwave (SW) component, the low, middle, and high cloud amount, and the cloud liquid and ice water path.

We have carefully examined various aspects of the simulated mean climate by each model to confirm that they perform comparably to those of earlier GFDL models as well as other CMIP5 models. Figures 2a and 2b show a comparison of the simulated longwave (LCRE) and shortwave CRE (SCRE) with 22 CMIP5 models (over the period 1981–2000, http://cmip-pcmdi.llnl.gov/cmip5/data_portal.html) forced by observed SSTs as well as the observational estimates derived from the NASA Clouds and the Earth's Radiant Energy System (CERES; EBAF Ed2.6 data over the period 2000–12, http://ceres.larc.nasa.gov/order_data.php; Smith et al. 2011). The latitudinal distributions of LCRE and SCRE from H, M, and L are close to the CERES estimates and are well within the spread of the CMIP5 ensemble. Figure 2c further compares these three models with the CMIP5 ensemble using the normalized root-mean-square errors (RMSEs) for seven selected fields: LW, SW, total CRE, surface precipitation, near-surface air temperature over land, sea level pressure, and surface zonal wind stress. The simulation qualities from H, M, and L are generally as good as or better than most CMIP5 models for most fields.

To assess the models' cloud feedback and climate sensitivity, we follow the Cess approach by conducting a pair of present-day and global warming simulations for each model using prescribed SSTs and greenhouse gas (GHG) concentrations (Cess et al. 1990). The present-day simulations are forced by the observed HadISST climatological SSTs averaged over the period of 1981–2000, with GHG concentrations fixed at the year 2000 level. The global warming experiments are identical to the present-day simulations, except SSTs are uniformly increased by 2 K. A Cess climate sensitivity parameter λ can then be computed as $\lambda = \Delta T_s/\Delta G$, where T_s denotes global mean SST, G is TOA net radiative flux, and Δ indicates the difference between warming and present-day simulations (Cess et al. 1990). The effect of clouds on λ can be measured by the ratio of the all-sky λ to clear-sky λ_{clr} sensitivity or by the changes in total CRE (TCRE), where $\lambda/\lambda_{\mathrm{clr}} = \Delta\mathrm{TCRE}/\Delta G + 1$ [see Eq. (9) in Cess et al. (1990); note, ΔG denotes their G]. Although the sign of ΔTCRE should not be simply interpreted as the sign of cloud feedback when ΔTCRE is modestly negative (Soden et al. 2004), ΔTCRE is strongly correlated across models with the cloud feedback computed using a more detailed partial radiative perturbation (PRP) method (Wetherald and Manabe 1988) or the kernel method (Soden and Held 2006). Cloud feedback computed by the kernel method is systematically more positive than ΔTCRE because of cloud masking ($\sim$0.3 $\mathrm{W\,m^{-2}\,K^{-1}}$ for Cess feedbacks), but the offset is roughly model independent (Soden et al. 2004).

Another simplification of the Cess approach is the use of uniformed SST warming experiments with an atmospheric-only model for studying cloud feedback.

TABLE 1. A list of the parameters used in the convective precipitation schemes in H, M, and L models and some of their simulated global quantities. See text for the definition of the parameters. The global quantities include the Cess climate sensitivity parameter, TOA total CRE and its LW and SW component, the low, middle, and high cloud amount, the cloud liquid and ice water path, and the precipitation.

Parameters used	H	M	L
q_0 (g kg^{-1})	1.5	0.8	0.8
T_{crit} (°C)	−90	—	—
β_l (Pa^{-1})	—	1.5×10^{-5}	4.0×10^{-5}
β_i (Pa^{-1})	—	3.0×10^{-5}	8.5×10^{-5}
α	—	4	1
Model-simulated global quantities			
Cess climate sensitivity (K W^{-1} m^2)	0.82	0.53	0.48
TOA TCRE (W m^{-2})	−24.2	−24.7	−24.8
TOA LCRE (W m^{-2})	25.9	24.7	23.8
TOA SCRE (W m^{-2})	−50.1	−49.4	−48.6
Low cloud amount (%)	37.0	36.3	34.7
Middle cloud amount (%)	17.5	17.9	17.8
High cloud amount (%)	37.7	36.4	36.1
Liquid water path (g m^{-2})	47.1	47.9	47.3
Ice water path (g m^{-2})	50.0	43.4	47.0
Precipitation (mm day^{-1})	3.00	3.00	3.01

Previous studies demonstrated that the cloud feedbacks derived from the Cess experiments well capture the intermodel differences of feedbacks in the equilibrium response of slab ocean models to a doubling of CO_2 (e.g., Ringer et al. 2006). Very recently, Ringer et al. (2014) and Brient et al. (2015) analyzed the CMIP5 fully coupled ocean–atmosphere models and their corresponding Cess experiments and confirmed again that the Cess experiments provide a good guide to the global cloud feedbacks determined from the coupled simulations, including the intermodel spread. The differences in total climate feedback parameter between the Cess and coupled models arise primarily from differences in clear-sky feedbacks that are anticipated from the nature of the Cess experimental design (i.e., ignoring the polar amplification and sea ice albedo feedback). As a result, the Cess climate sensitivity parameter should not be interpreted at its face value for estimates of model equilibrium climate sensitivity. With these limitations in mind, the Cess approach has been widely used in characterizing and understanding many aspects of intermodel differences in cloud feedback and climate sensitivity between GCMs (e.g., Cess et al. 1990; Zhang et al. 1994; Cess et al. 1996; Soden et al. 2004; Wyant et al. 2006; Ringer et al. 2006; Bony et al. 2006; Medeiros et al. 2008; Wyant et al. 2009; Brient and Bony 2012, 2013; Bretherton et al. 2014; Ringer et al. 2014; Webb et al. 2015). It is because of its high relevancy as well as its much lower computational cost that the Cess-like experiments have now become a standard set of simulations requested by the IPCC Cloud Feedback Model Intercomparison Project (CFMIP) and continue to serve as an important tool for studying intermodel difference in cloud feedback.

3. Results

A scatterplot of the Cess climate sensitivity parameter λ versus the cloud feedback parameter ΔTCRE/ΔG from H, L, and M is shown in Fig. 3a. For comparison, AM2, AM3, and HiRAM results are also plotted. The value of λ ranges from 0.48 K m^2 W^{-1} in L to roughly 0.82 K m^2 W^{-1} in H with a large intermodel spread well accounted for by changes in the cloud feedback parameter. This result is consistent with many earlier studies that show that spread of equilibrium climate sensitivity among GCMs is primarily due to model differences in cloud feedback. The deviation of AM3 sensitivity from the regression line in Fig. 3a is largely caused by its clear-sky sensitivity parameter λ_{clr} being about 0.08 K m^2 W^{-1} lower than the other models for reasons not yet clear. Except for AM3, all other models fall nicely along a straight line with both the intercept and the slope of the linear regression close to the models' direct estimates of λ_{clr} ($\sim$0.55 K m^2 W^{-1}).

The intermodel variations in changes of total CRE are well explained by model difference in response of convective detrainment efficiency κ_c, as shown in Fig. 3b. The three models (H, HiRAM, and AM3) with large positive cloud feedbacks also exhibit larger reductions in κ_c, while the diminished positive cloud feedbacks in AM2 and M and the negative cloud feedback in L are associated with little change or an increases in κ_c. This result suggests that changes in cumulus detrainment efficiency are important in understanding the response of total CRE with warming in these models.

Z14 conjectures that the different assumptions in representing cumulus precipitation may be partly responsible for the increased positive cloud feedback in HiRAM and AM3 compared to AM2. Since the convection schemes in AM2, AM3, and HiRAM differ not only in precipitation treatment but also in many other important aspects (e.g., number of plumes, mixing characteristics, and cloud-base mass flux closure), it was impossible for Z14 to preclude other possibilities. However, the set of AM4 models (H, M, and L) provides clean evidence that assumptions in cumulus precipitation alone can strongly alter cloud feedback and climate sensitivity in a GCM, and the impact may be understood through an aggregated bulk parameter κ_c.

The tightly controlled H, M, and L models provide us clean cases to understand why the differing assumptions in cumulus precipitation lead to large discrepancies in

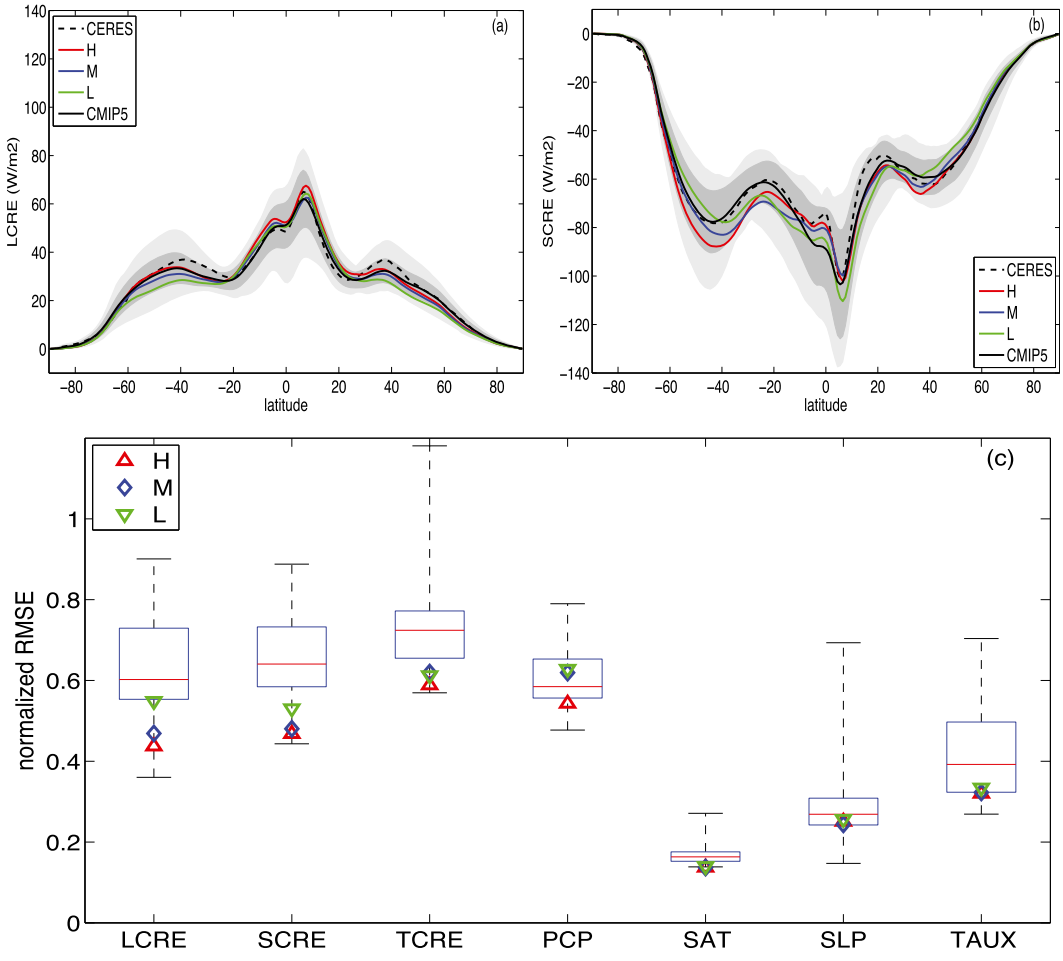

FIG. 2. (a) A comparison of the latitudinal distribution of LCRE between H, M, L, 22 CMIP5 models forced by observed SSTs, and the observational estimates from CERES (EBAF Ed2.6). The black solid line shows the ensemble mean of the 22 CMIP5 models with dark shading for one standard deviation and light shading for minimum and maximum values. (b) As in (a), but for the SCRE. (c) A comparison of normalized RMSEs for seven selected fields between H, M, L, and the 22 CMIP5 models (shown in box-and-whisker plots: center markers are medians, bottom and top box edges are 25th and 75th percentiles, and whiskers are minimums and maximums). Each model's RMSEs are computed from the global distribution of annual mean biases between a model and observations. The RMSEs for each field are normalized by the standard deviation of spatial variation of the observed annual mean field so that different fields can be shown in one plot. The observational data used here are respectively CERES (EBAF Ed2.6) for LCRE, SCRE, and TCRE; GPCP (version 2.2, 1981–2010, http://www.esrl.noaa.gov/psd/data/gridded/data.gpcp.html) for surface precipitation (PCP); Hadley Centre/Climatic Research Unit temperature dataset, version 3 (HadCRUT3 ; 1981–2000, http://www.metoffice.gov.uk/hadobs/hadcrut3/), for 2-m surface air temperature (SAT) over land; ECMWF interim reanalysis data (ERA-Interim; 1979–2011, http://www.ecmwf.int/en/research/climate-reanalysis/era-interim) for sea level pressure (SLP), and surface zonal wind stress (TAUX). The legend shows symbols for H, M, and L.

cloud feedback. Figure 4a shows changes in LCRE, SCRE, and TCRE between the SST warming and the present-day simulations. Globally, H produces $0.57\,\mathrm{W\,m^{-2}\,K^{-1}}$ increase (less negative) in TCRE, which is contributed by a larger increase (less negative) in SCRE with a small compensation through a reduction in LCRE. In contrast, M produces a small net reduction ($-0.1\,\mathrm{W\,m^{-2}\,K^{-1}}$) in TCRE because of a significant reduction ($-0.2\,\mathrm{W\,m^{-2}\,K^{-1}}$) in SCRE and a small increase in LCRE. Moreover, L produces a larger reduction (more negative; $-0.38\,\mathrm{W\,m^{-2}\,K^{-1}}$) in TCRE, which is composed of $-0.59\,\mathrm{W\,m^{-2}\,K^{-1}}$ reduction in SCRE and a modest compensation increase in LCRE. It is clear that the differences in TCRE response between the models are dominated by their SW component, with their LW component tending to counteract some of their SW responses. This result is consistent with many earlier studies of the importance of SW feedbacks for model spreads, including the more recent CMIP5 analyses (e.g., Donohoe et al. 2014; Vial et al. 2013). The model

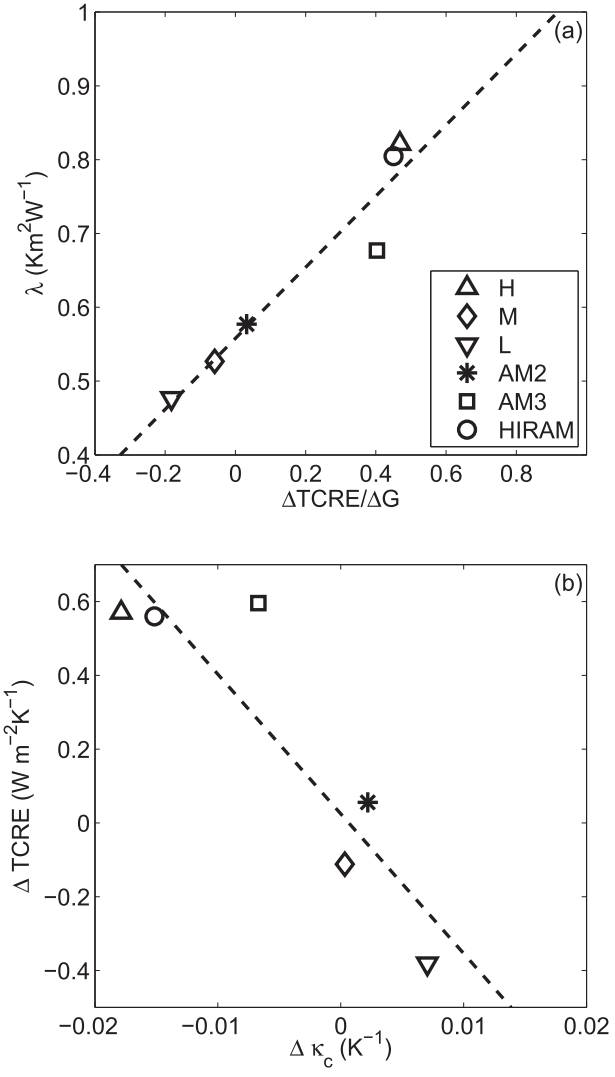

FIG. 3. (a) Scatterplot of the Cess climate sensitivity parameter λ vs cloud feedback parameter $\Delta\text{TCRE}/\Delta G$ from H, M, L, AM2, AM3, and HiRAM. See text for the definitions of TCRE, G, and Δ. The dashed line shows linear regression. (b) As in (a), but for changes in TCRE vs changes in convective detrainment efficiency κ_c (see Fig. 1). All changes are for the global means and normalized per kelvin of warming.

contrasts become stronger for the tropical means (Fig. 4a), suggesting that the global mean differences are dominated by the tropics, as is confirmed by direct inspection of the latitudinal dependence of these changes (not shown).

Figure 4b shows that, as the climate warms, global mean liquid and ice water contents tend to increase while cloud amounts or fractions decrease, with low-plus-middle cloud fractions (below 400 hPa) diminishing more prominently than the high cloud fraction (e.g., Stephens and Ellis 2008). Clouds on average tend to be denser and less frequent in warmer climate in all the models. However, the magnitude of reductions in low-plus-middle cloud fractions in H is considerably larger than that in M and L. Meanwhile, the magnitude of global increases in liquid and ice condensate is smaller in H than in M and L. Both are consistent with their different response in SCRE. The contrast becomes especially clear in the tropics where the percentage change in low-plus-middle cloud fraction is reduced from roughly $-13\%\,\text{K}^{-1}$ in H to roughly $-3.5\%\,\text{K}^{-1}$ in M and L. Consistently, the response in liquid and ice water paths changes from $-1.5\%\,\text{K}^{-1}$ in H to $+3\%$–$5\%\,\text{K}^{-1}$ in M and L in the tropics. Despite the significant differences in cloud response, changes in global mean precipitation show very little difference between the models, which may be partly due to the limitation of the Cess experiment (i.e., SSTs are prescribed). Both the weaker reductions in low-plus-middle cloud fractions and the enhanced gains in cloud condensate path (which are dominated by low- and middle-level clouds) from H to M and L are important in explaining the differences in cloud feedback from strongly positive in H to relatively neutral in M and slightly negative in L.[1]

Since the differences in global mean cloud responses between the models are dominated by the tropics, below we focus on the tropical region (30°S–30°N) to examine the intermodel differences. We first show the vertical profiles of cloud fraction and cloud condensate averaged over the entire tropical ocean in Figs. 5a and 5b. The largest differences between the models appear to be in the middle troposphere between 400 and 800 hPa, with H producing fewer midlevel clouds and slightly more high clouds for both cloud fraction and condensate. This result is consistent with recent findings by Webb et al. (2015) and Brient et al. (2015), who show that the high-sensitivity models in the CMIP5 ensemble also tend to have fewer midlevel clouds. Figures 5c and 5d further show the change in vertical profile of cloud fraction and condensate between the warmer and the present-day simulations. Interestingly, the largest differences in cloud response are also below 400 hPa, with the higher-level cloudiness showing a robust dipole pattern, indicating an upward shift of high-level cloud in a warmer climate (Hartmann and Larson 2002). Below 400 hPa, H produces systematically larger reductions of cloud throughout the middle and lower troposphere, while M and L produce a minimal reduction of cloud below 600 hPa and even an increase above. The intermodel differences in response of both cloud cover and condensate amount are consistent with

[1] This statement has taken into account the $0.3\,\text{W m}^{-2}$ difference between the ΔTCRE metrics and the radiative kernel metrics (Soden et al. 2004).

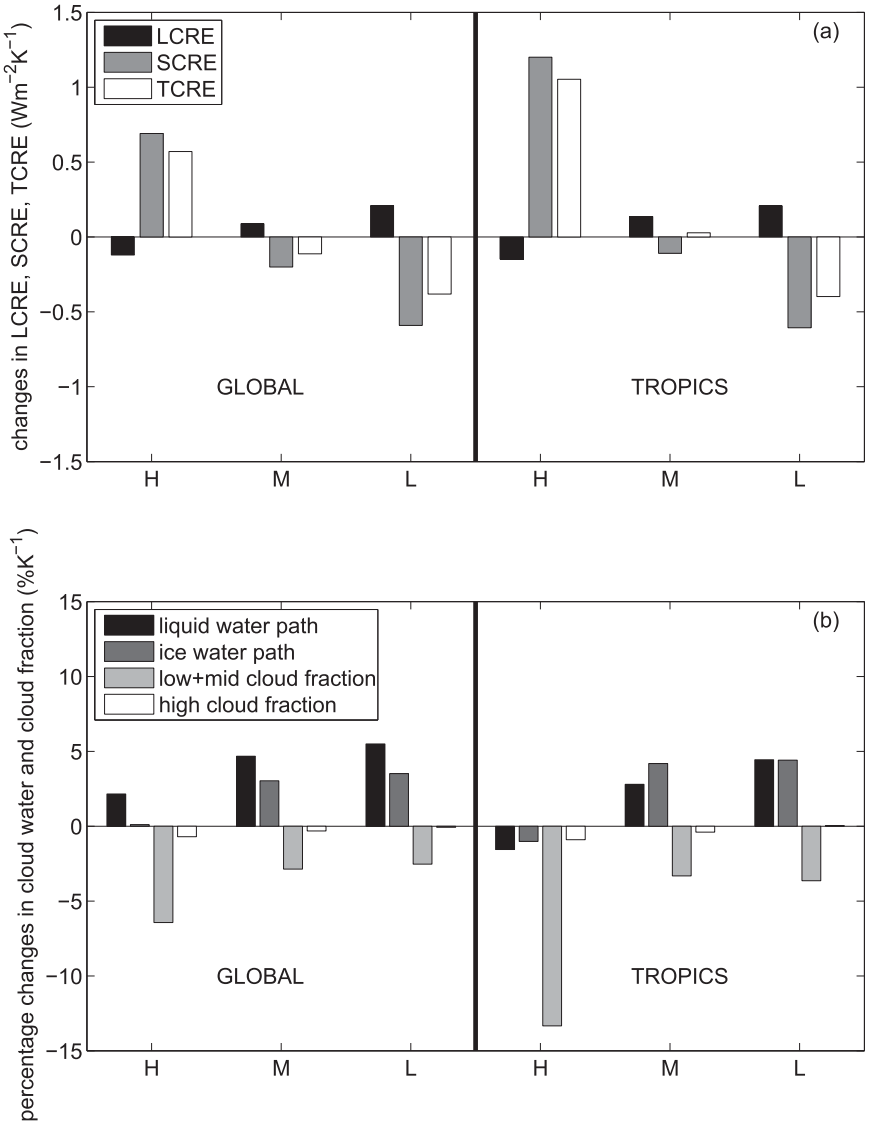

FIG. 4. (a) Changes in LCRE, SCRE, and TCRE from H, M, and L for both the global and the tropical (30°S–30°N) means. Units are normalized per kelvin of warming. (b) As in (a), but for fractional changes in liquid and ice water paths, low-plus-middle (below 400 hPa), and high (above 400 hPa) cloud fractions.

their differences in tropical mean CRE response. In addition, the negative feedback due to phase change of middle-level clouds from ice to liquid should contribute to the reduction of positive cloud feedback in M and L since they contain more midlevel clouds. Below, we further partition the tropical mean CRE changes into different large-scale regimes to explore what regimes might best explain their tropical mean responses.

We follow the Bony method (Bony et al. 2004; Bony and Dufresne 2005) by sorting changes in tropical CREs into different regimes of large-scale overturning circulation characterized by monthly mean 500-hPa vertical pressure velocity ω_{500}. Figures 6a–c show changes in LCRE, SCRE, and TCRE across all ω_{500} regimes. Consistent with the global means, changes in the SW component dominate the total CRE changes, while the LW component tends to slightly oppose the SW effects. Large differences in SCRE response between the three models do not only occur over the large-scale ascent regions but also extend throughout the subsidence regions, indicating that the tropical mean differences in SCRE response are contributed from a wide range of regimes, from deep cumulonimbus to cumulus congestus and shallow cumulus clouds in these models.

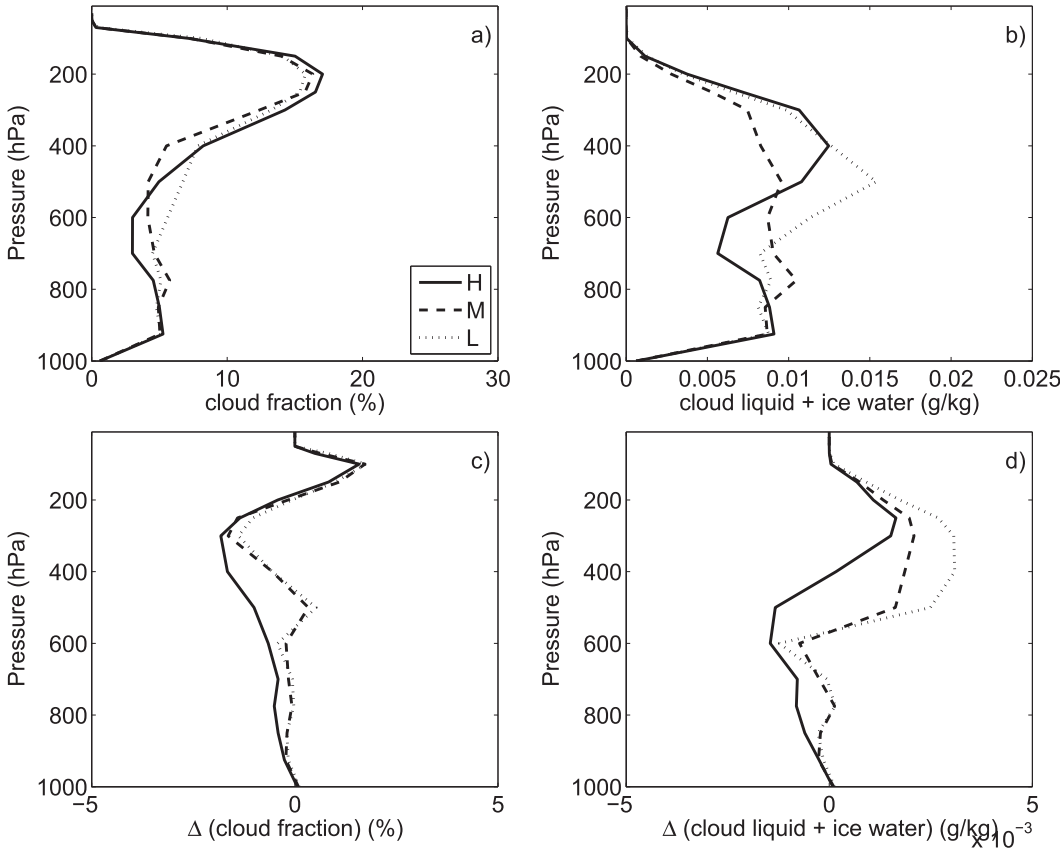

FIG. 5. (a) Vertical profiles of cloud fraction averaged over the tropical (30°S–30°N) ocean from H, M, and L. (b) As in (a), but for cloud condensate (liquid + ice). (c) As in (a), but for the change in cloud fraction between warmer and present-day simulations. (d) As in (c), but for cloud condensate.

Except in the very strong ascent regions ($\omega_{500} < -80\,\text{hPa day}^{-1}$), H produces positive changes in SCRE across all other ω_{500} regimes. In contrast, M and L produce negative SCRE responses in all tropical large-scale ascent regions and gradually transition to positive responses in some subsidence regions. Throughout all regimes, H produces systematically the largest changes (more positive or less negative) in SCRE, while L generates the smallest changes (more negative or less positive), with M generally in the middle. The intermodel differences in SCRE and TCRE response are larger in the broad ascent regimes with either strong or marginal precipitation. However, their global mean differences are dominated by the weakly ascending and subsiding regions because of their larger spatial coverage (Bony et al. 2004; Bony and Dufresne 2005). This can be seen from the changes in TCRE, weighted by the tropical probability density function (PDF) of ω_{500} computed from each model's present-day simulation (Fig. 6d).

The model differences in SCRE response can be understood from their differences in simulated changes in low and middle clouds. Figure 7a shows that, for all regimes, H produces systematically more reductions in low-plus-middle cloud amounts than M and L. In addition, H also produces the least increases in liquid and ice water path in the ascent region (Fig. 7b). Over the subsidence regions, H generates reductions in liquid water path in contrast to little changes or increases in M and L (Fig. 7b). Both the smaller reductions in low-plus-middle cloud fractions and the larger increase in cloud condensate path (optical depth) are important for the negative cloud feedback in M and L compared to the positive feedback in H.

Previous studies based on the model results from phase 3 of CMIP (CMIP3) showed that the regimes of weak subsiding motion tend to dominate the intermodel spread in cloud feedback because of their larger spatial coverage (Bony and Dufresne 2005). Recent analysis by Vial et al. (2013) suggested that, compared to the CMIP3 models, the spread of tropical cloud feedbacks between the CMIP5 models arises from a larger range of dynamical regimes, ranging from weak large-scale ascent motions to subsidence regimes. These results are, in general, consistent with our findings, which also suggest that, in addition

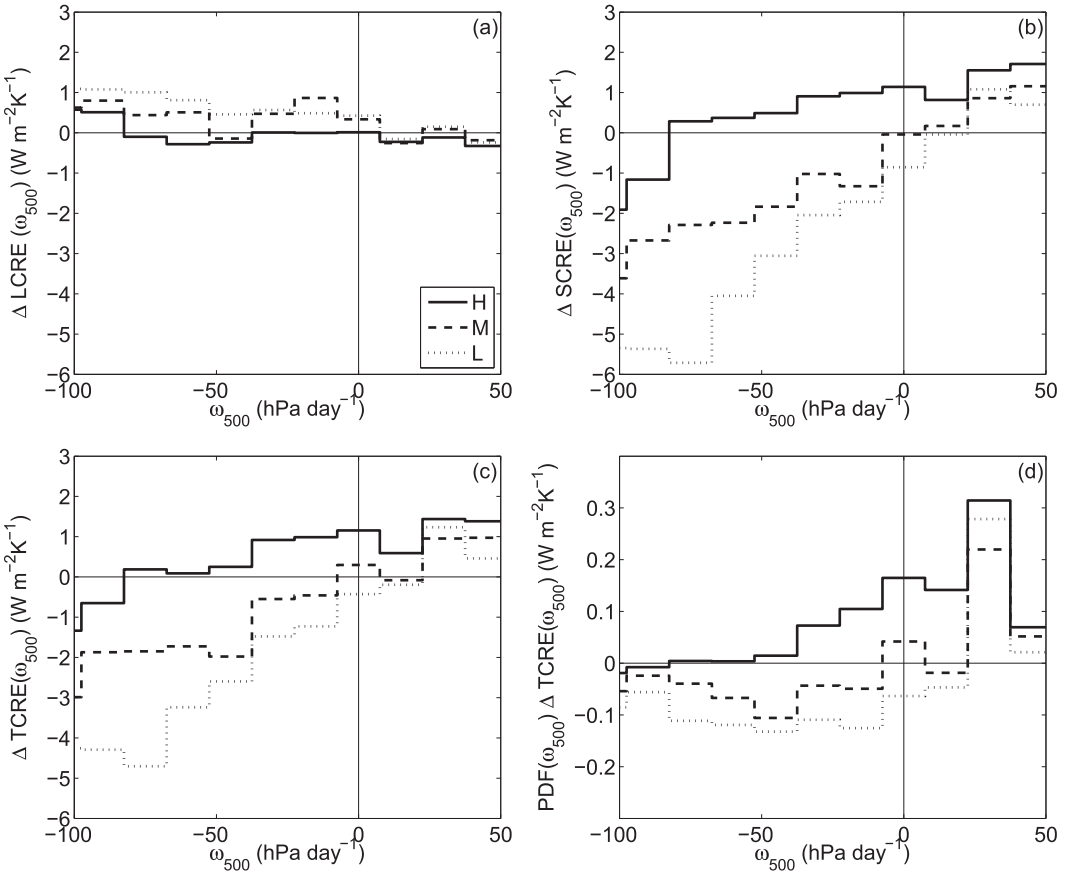

FIG. 6. Changes between warmer and present-day climates for tropical (30°S–30°N) mean LCRE, SCRE, and TCRE sorted into different large-scale regimes characterized by monthly ω_{500}: (a) ΔLCRE(ω_{500}), (b) ΔSCRE(ω_{500}), and (c) ΔTCRE(ω_{500}). (d) As in (c), but ΔTCRE(ω_{500}) is weighted by each model's present-day PDF of ω_{500}.

to the weak subsidence regime, the response of low and middle clouds over the broad ascent regimes can also exert large impacts on global cloud feedbacks. Our results demonstrate that the differing assumptions commonly used in representing convective precipitation can strongly affect cloud response across both ascending and descending large-scale regimes in a GCM and, through this, impact model estimates of cloud feedback and climate sensitivity since that is the only difference between H, M, and L.

To understand why the threshold removal scheme used in H produces a marked increase in positive cloud feedback compared to the fractional removal schemes in M and L, we compute fractional changes in convective detrainment efficiency κ_c for each ω_{500} regime. Figure 8a shows that, for all regimes, H produces either more reduction or less increase in $\Delta\kappa_c/\kappa_c$ with warming compared to M and L. As the climate warms and in the absence of precipitation, cumulus cloud condensate would increase at a rate determined by the change in the moist adiabatic lapse rate (Betts and Harshvardhan 1987). A fixed threshold removal scheme would convert all the additional condensate into precipitation, resulting in a large decline in detrainment efficiency. While the condensate threshold for precipitation q_{c0} is not precisely fixed with warming in H [it slightly increases for cold clouds with temperature between 0°C and T_{crit} as a result of the formulation (Emanuel and Zivkovic-Rothman 1999)], its effect is small, and to the first order H behaves like a fixed threshold removal scheme.

Alternatively, as the climate warms, the tropical mean convective mass flux decreases despite increases in precipitation (Held and Soden 2006). A fixed threshold removal scheme would lead to a decrease in total convective detrainment because the condensate mixing ratio in detrained cloudy air is kept fixed, and all additional condensate is simply removed as precipitation. However, to maintain the same supersaturation (or cloudiness) in a warmer climate with fixed relative humidity (a good assumption to first approximation), one would need an increase in condensate detrainment following the Clausius–Clapeyron relation (Rieck et al. 2012). Thus, everything

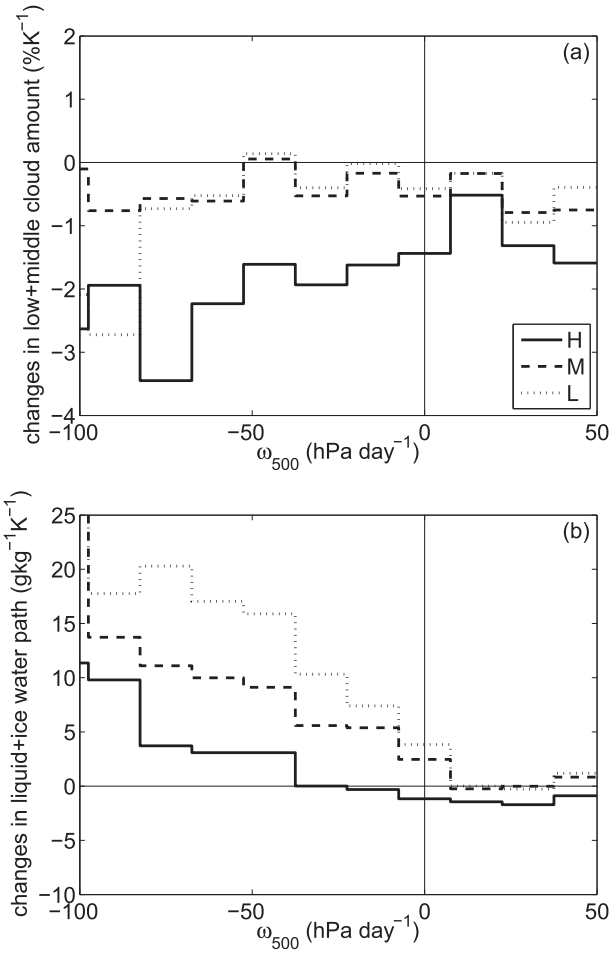

FIG. 7. Changes in (a) low-plus-middle (below 400 hPa) cloud amount and (b) liquid and ice water path between warmer and present-day simulations computed for different tropical large-scale ω_{500} regimes.

else being equal, such a decrease in convective detrainment would lead to an enhanced reduction in cloudiness. The reduction in convective detrainment tends to diminish low and middle clouds more strongly because the decreases in convective mass flux are larger over the lower and middle troposphere. Compared to M and L, the stronger reductions in convective detrainment efficiency in H lead to substantially larger decreases in low and middle clouds (especially cloud amount) and their reflection of sunlight, enhancing their positive cloud feedbacks and Cess climate sensitivity.

In contrast to the threshold removal scheme, a fractional removal scheme can result in substantial increases in cumulus condensate mixing ratio with warming, especially for midlevel clouds with relatively cold temperature (Somerville and Remer 1984; Betts and Harshvardhan 1987). This condensate is eventually detrained into the troposphere, counteracting the effect of decreasing convective mass flux by lessening the reduction of low-plus-middle cloud amount and increasing the liquid and ice water path (Fig. 7). Indeed, Fig. 8a shows that L and M produce systematically less negative or more positive changes of κ_c than H, resulting in little reduction (M) or even an increase (L) in the tropical bulk convective detrainment efficiency (Fig. 3b). This is ultimately responsible for their neutral-to-negative cloud feedback and lower Cess climate sensitivity.

Since the total convective detrainment of condensate is $C_c - P_c = \kappa_c P_c$ and $\Delta(\kappa_c P_c) \approx \kappa_c \Delta P_c + P_c \Delta\kappa_c$, the change in κ_c is not the only factor that can affect the response in the convective detrainment. The change in the convective precipitation P_c can also play a role. Figures 8b–d shows this partition into the component due to changes in convective precipitation P_c and the component due to $\Delta\kappa_c$. In the regions of most extreme ascent, the ΔP_c term dominates the total response and produces overall increases in total detrainment. However, the intermodel differences in total detrainment are primarily caused by their difference in $\Delta\kappa_c$, especially over the broad weak ascent and decent regions, which dominate the tropical and global mean response. Figure 8d also shows that, even in the subsidence regions with much smaller precipitation rate, changes in κ_c can still significantly affect the response of convective detrainment. Since cumulus detrainment in subsidence regions tends to be confined in a lower troposphere where it is warmer, the impact on cloudiness for the same amount of condensate would be smaller than that detrained at a higher level in ascent regions following Clausius–Clapeyron. Nevertheless, the significant effect of precipitation over a large area of subsidence regions makes the response of κ_c important in both ascent and descent regions.

In the subsidence regions, it is also interesting to note that convective precipitation tends to decrease, which counteracts the increases in $\Delta\kappa_c$ and produces smaller changes in detrainment of condensate. While the intermodel differences in $\Delta\kappa_c$ are consistent with their differences in cloud response (see Fig. 6), the overall positive $\Delta\kappa_c$ in the subsidence regions alone would not explain the broad reduction of low clouds there. This suggests that other processes shared between the models may be important in explaining the overall reduction in low cloud amount in the subsidence regions. This is not surprising since low-cloud responses in the subsidence regions are affected not only by changes in cumulus detrainment but also by various processes closely related to the planetary boundary layer turbulence, a topic beyond the scope of the current paper.

4. Summary and discussion

Poor understanding of cloud feedback is a leading cause of disagreement in GCM predictions of future

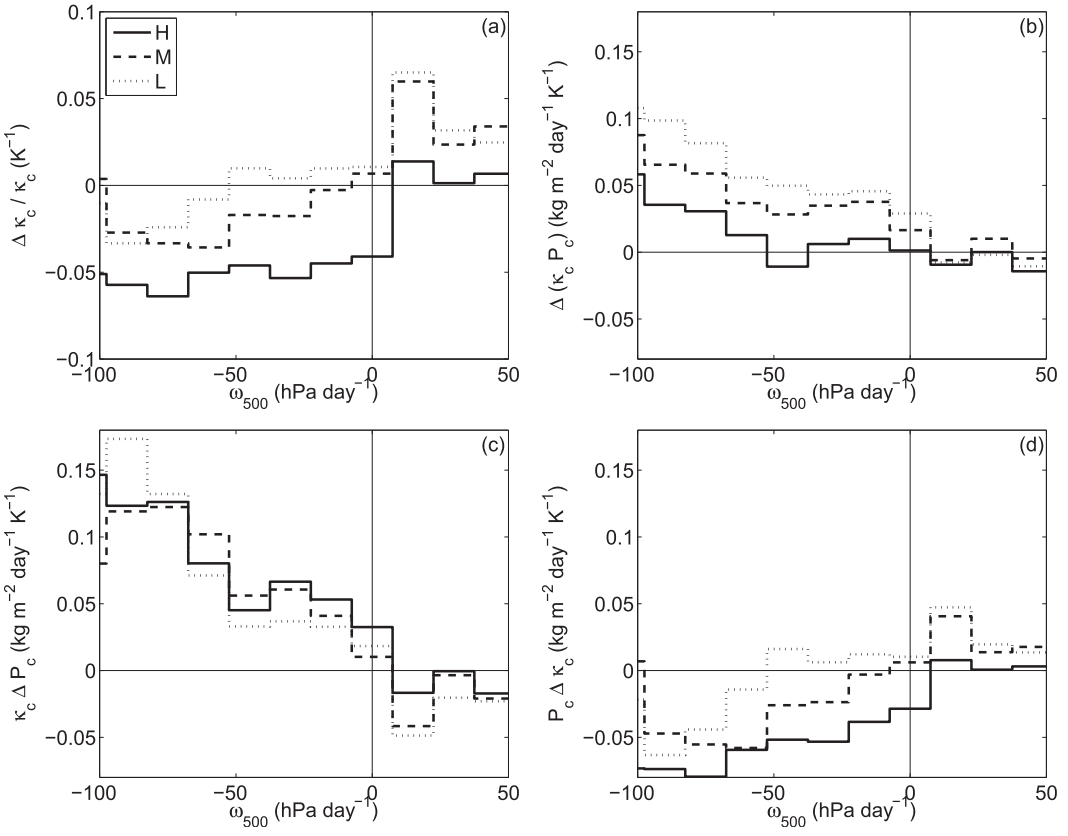

FIG. 8. (a) Fractional changes in convective detrainment efficiency κ_c computed for different tropical large-scale ω_{500} regimes. (b) As in (a), but for changes in the rate of total convective detrainment of liquid and ice water $\Delta(\kappa_c P_c)$. (c) As in (b), but for the component due to changes in ΔP_c ($\kappa_c \Delta P_c$). (d) As in (b), but for the component due to changes in $\Delta\kappa_c$ ($P_c \Delta\kappa_c$). All changes are computed over the tropics and normalized per kelvin of warming.

climate. Despite being aware of the problem for some time, we are now beginning to develop specific ideas that lend themselves to a variety of tests (e.g., Bony et al. 2015; Mauritsen and Stevens 2015; Sherwood et al. 2014; Z14; Stevens and Bony 2013). Here we show that model estimates of cloud feedback can be strongly affected by the manner through which cumulus cloud condensate is converted into precipitation in a model's convection parameterization. Based on a developmental version of the next-generation GFDL GCM (AM4), we have created three models that are identical in all aspects of the dynamics and physics formulations except the treatment of cumulus precipitation. Without impacting the quality of the simulated climate appreciably, we demonstrate that the two commonly used methods for parameterizing convective precipitation can result in drastically different cloud feedbacks, with the threshold removal scheme (H) producing a strong positive feedback and the fractional scheme (M and L) generating neutral to slightly negative feedbacks.

The effect can be understood through a bulk convective detrainment efficiency, which measures the ability of cumulus convection to generate clouds and moisten the free troposphere per unit precipitation (Z14). The analysis of clouds and convective detrainment efficiencies from different large-scale dynamical regimes characterized by ω_{500} suggests that the difference in simulated global and tropical mean cloud response comes from broad regimes ranging from strongly ascending to weakly ascending to weakly descending, corresponding to deep cumulonimbus, cumulus congestus, and shallow cumulus cloud regimes in these models. This result is broadly consistent with recent findings by Vial et al. (2013), who showed that the difference in tropical cloud feedbacks between the high- and low-sensitivity CMIP5 models arises from a larger range of dynamical regimes (from ascent to subsidence regimes).

Although this study suggests that the response of convective detrainment (or precipitation) efficiency to global warming may be important for understanding GCM-simulated cloud feedback uncertainties, it is beyond the goal of the present paper to answer how convective precipitation may change in a warmer climate. Many processes can affect the convective precipitation

efficiency, including cumulus mixing dynamics, the formation and evolution of cloud and precipitating hydrometeors, the fall of precipitation and associated downdrafts, and precipitation reevaporation, as well as convection organization and its interactions with radiation and circulation. High-resolution cloud-resolving simulations of radiative–convective equilibrium (RCE) suggest that convection is more likely to aggregate in a warmer climate (e.g., Emanuel et al. 2013). This suggests a possible increase in precipitation efficiency with warming. However, model simulations of convective aggregation in RCE are sensitive to many details, including domain size, resolutions, and initial conditions (e.g., Bretherton et al. 2005; Muller and Held 2012). Coupled with our limited understanding of the relevance of RCE for more realistic atmosphere, the relevance of this result for climate sensitivity remains unclear.

Once aggregated, the organized convection tends to dramatically reduce the domain-averaged relative humidity and clouds throughout the troposphere, indicating strong reductions in the magnitude of both LW and SW CRE (e.g., Bony et al. 2015; Tobin et al. 2012). It is, however, not obvious how the net CRE might change because of the cancellation between LW and SW components, especially considering the poor simulation of thin cirrus clouds in current GCMs, which could have a large impact on LW CRE. Recently, Mauritsen and Stevens (2015) hypothesized that a possible increase in convection aggregation in warmer climates might lead to the iris effect of Lindzen et al. (2001), which could be missing in GCMs and may cause the high climate sensitivity and muted hydrological change in GCMs. However, changes in precipitation efficiency in our model do not appear to manifest themselves as a significant iris-like effect. As shown in Figs. 4–6, the models produce a much smaller difference in the response of high clouds and LW CRE than the response of low-plus-middle clouds and SW CRE. At this time, it is not clear to what extent the iris effect due to changes in precipitation efficiency might be model dependent, but there is an indication that this might be the case. As pointed out by Mauritsen and Stevens (2015), when their formulation [Eq. (1) in Mauritsen and Stevens (2015)] for parameterizing convective precipitation efficiency is used in the NCAR climate model, it produces an increase in equilibrium climate sensitivity opposite to the decrease seen in the ECHAM6 model. Future research would be needed to understand the cause of these discrepancies.

In addition to convective precipitation microphysics, previous studies point out that changes in cumulus mixing or entrainment rate can also affect model estimates of cloud feedback and climate sensitivity (e.g., Murphy et al. 2004; Stainforth et al. 2005; Sanderson et al. 2008; Joshi et al. 2010; Sherwood et al. 2014; Z14). Z14 suggests that some of the effect of cumulus mixing can be understood through the convective detrainment efficiency since cumulus mixing directly affects the convective precipitation and therefore the detrainment efficiency. However, alterations of cumulus mixing rate strongly interact with other components of GCM physics, including the amount of resolved or explicit convection and the planetary boundary layer turbulence, both of which can profoundly affect GCM-simulated mean climates. For example, Held et al. (2007) showed that an increase in the cumulus entrainment rate limiter in GFDL AM2 strongly increases the fraction of tropical precipitation that comes from the resolved convection. This results in a significantly drier and warmer tropical troposphere with excessive boundary layer clouds and SW reflection at TOA. These effects can be seen in both GCM simulations and idealized RCE simulations using GCM physics (Held et al. 2007). The large TOA radiative imbalance often requires significant retuning outside of the convection scheme. Moreover, because the explicit convection plays a significant role in tropical convective transport and precipitation, an appreciation of the response of total detrainment efficiency would require an understanding of the precipitation efficiency in the explicit (resolved scale) cloud module, which should depend on the formulation of explicit cloud microphysics.

The complicated impacts of cumulus mixing on other components of GCM physics often make it challenging to isolate and understand the mechanisms through which cloud feedbacks are changed. As an example of this complexity, Joshi et al. (2010) found that the high climate sensitivity in one version of the Met Office Hadley Centre single-parameter perturbed physics model (Murphy et al. 2004) with low entrainment parameter is due to stratospheric humidity change, rather than the upper-tropospheric clouds suggested by previous studies.

Based on an analysis of the simulations from 43 GCMs participating in the CMIP3 and CMIP5, Sherwood et al. (2014) suggest that the model spread in climate sensitivity is caused mostly by the tropical low-cloud response due to intermodel variations in convective mixing strength between the lower and middle troposphere. Based on the mixing inferred from observation and reanalysis data, they suggest that the models with higher climate sensitivity may be more realistic for predicting future global warming.

The mechanism that Sherwood et al. (2014) put forward is that the mixing between the lower and middle troposphere tends to dehydrate the low cloud layer at a rate that increases as the climate warms, and this rate

of increase depends on the initial mixing strength. They suggest that a model with stronger present-day mixing strength, as measured by their index of subgrid-scale mixing S and an index of large-scale mixing D [see Sherwood et al. (2014) for the definitions of S and D], tends to produce more positive cloud feedback and therefore a higher sensitivity. We have made the same calculation of these indices from H, M, and L and found no evidence that these indices explain the model differences described here. In particular, we found S to be systematically larger in the lower-sensitivity models M and L than in H. Moreover, both D and the sum of S and D do not show a good correlation with cloud feedback or the Cess climate sensitivity parameters. Table 2 provides the values for the S and D indices computed from each of the models.

TABLE 2. The S, D, and $S + D$ indices of Sherwood et al. (2014) computed from the H, M, and L models. See Sherwood et al. (2014) for the definition of the parameters.

Parameters	H	M	L
S	0.44	0.46	0.47
D	0.28	0.24	0.27
$S + D$	0.72	0.70	0.74

The fundamental picture behind Sherwood et al. (2014) is that an increase of upward transport of moisture near the top of the boundary layer over the convective regions should result in decrease of low clouds because of dehydration of the boundary layer (Rieck et al. 2012). To understand whether this mechanism might be operative in our models even though the specific indices discussed by Sherwood et al. (2014) do not correlate with climate sensitivity as proposed, we have directly computed the net upward flux of total water (vapor plus liquid plus ice) at each model level over the tropics. This net flux is the sum of the net total water fluxes due to the parameterized and resolved-scale convection and the boundary layer turbulence. Resolved-scale water flux is computed online based on upward vertical pressure velocity at each physics time step of a model.

Figure 9 shows the changes in the total water flux between the warmer and present-day climate. It is clear that the two low-sensitivity models (M and L) produce a larger increase in upward water flux near the top of the boundary layer (800–900 hPa) than the high-sensitivity model (H). While they may dehydrate the boundary layer more, most of the additional upward water flux is deposited between 800 and 400 hPa, which results in less reduction or even an increase of clouds in the middle levels well above the boundary layer. These clouds have a large SW radiative effect. Our results suggest that this effect depends strongly on the treatment of convective precipitation, and it can dominate the overall response of SW and total CRE in a GCM. Although our results provide an example that the mechanism described in Sherwood et al. (2014) cannot explain, this study alone would not suggest that the mechanism explored here and the convective detrainment efficiency can explain a large fraction of the intermodel spread in the CMIP5 models. Nevertheless, our results are consistent with Fig. 5 in Sherwood et al. (2014), which shows that considerable spread in climate sensitivity remains even for a fixed S, D, and $S + D$. In that sense, the present study is complementary to Sherwood et al. (2014) toward piecing together a complete understanding of the processes that result in the spread in climate sensitivity across GCMs.

Given the current level of uncertainty in representing convective precipitation microphysics, this study suggests that one can engineer climate sensitivity in a GCM by the approach used for parameterizing convective precipitation. The differences between the present-day mean climate simulations in the three models described here are modest, as shown in Fig. 2, with L performing a bit less well than H and M, but we suspect that by optimizing other areas of the model we could reduce some of these differences. So far, we have not found a clear constraint that we feel would make one model choice more plausible than another. Therefore, holistic measures of the overall quality of the mean climate simulations do not appear to provide adequate guidance for choosing between these models. To accelerate progress for understanding and constraining cloud feedback and climate sensitivity, comprehensive approaches are necessary. They would include 1) a thorough evaluation of GCM-simulated cloud variability at all temporal and spatial scales in addition to the mean climatology, 2) development of hypotheses (or story lines) around key questions and/or processes for models to confront (e.g., Bony et al. 2015), 3) process-oriented investigations using high-resolution cloud-resolving and large-eddy simulations (e.g., Bretherton et al. 2013, 2014), and 4) development and use of a global cloud-resolving model or superparameterized GCM for cloud feedback.

In addition, there is value in intentionally engineering climate sensitivities in specific ways in traditional GCMs so as to provide material for further research into possible observational constraints (e.g., Mauritsen and Stevens 2015). One important way to manipulate climate sensitivity, through the convective detrainment efficiency, seems, as described here, to be particularly powerful in this regard. Models with explicitly engineered climate sensitivity should also be valuable in studying other constraints on sensitivity from studies of paleoclimates, volcanic responses, and simulations of

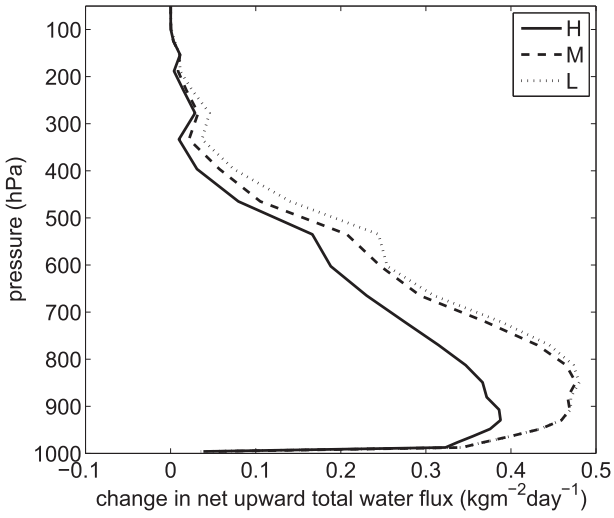

FIG. 9. Changes in vertical profile of net convective total water flux between warmer and present-day climate. The net flux is the sum of the total water (vapor + liquid + ice) fluxes due to the parameterized and resolved-scale convection and the boundary layer turbulence over the tropical convective regions. Resolved-scale water flux is computed online based on upward vertical pressure velocity at each physics time step of a model.

the warming over the past century. In the latter case, engineering models with different strengths of indirect aerosol effects (Golaz et al. 2013) will also be needed to search for the most powerful constraints provided by the historical record.

Acknowledgments. The authors are grateful for helpful comments and suggestions from Drs. Michael Winton, Rong Zhang, and Nir Benmoshe. Comments and suggestions from three anonymous reviewers have significantly improved the paper. This research is partially funded by NOAA's Climate Program Office, Climate Variability and Predictability Program (GC14-252). The findings are those of the authors and do not necessarily reflect the views of the National Oceanic and Atmospheric Administration or the U.S. Department of Commerce.

APPENDIX

A Description of the Convection Scheme

The convection scheme is adapted from the University of Washington Shallow Cumulus scheme originally developed by Bretherton et al. (2004). Some earlier modifications have been documented in appendix A of Zhao et al. (2009). The modified version has been used in GFDL HiRAM for the IPCC Fifth Assessment Report (AR5) high-resolution time-slice simulations and the intermodel comparison project for the U.S. Climate Variability and Predictability Program (CLIVAR) Hurricane Working Group (Walsh et al. 2015). Below, we describe the motivations and new modifications that we have made for the developmental version of AM4 used in this study.

Similarly to HiRAM, when the previous modified UWShCu convection (Zhao et al. 2009) was used in AM4 prototypes, we find the model produces high-quality simulations of mean climate and tropical cyclone statistics when the model is forced by the observed SSTs. However, when coupled with an ocean model (MOM5), we find it produces too-strong equatorial Pacific code biases, which negatively affect model simulations of El Niño–Southern Oscillation (ENSO). In addition, the model produces signals of the Madden–Julian oscillation (MJO) that are too weak and do not propagate into the western tropical Pacific. We suspect that this may be caused by some deficiencies in the model's representation of deep convection since the original scheme was designed for shallow cumulus clouds, and our simple adjustment of the fractional lateral mixing rate ε to a smaller value [i.e., c_0 was adjusted to be 10 in Zhao et al. (2009) instead of 15 in Eq. (18) of Bretherton et al. (2004)] may not fully account for the effect of deep convection.

In an attempt to reduce these coupled biases, we introduce an additional bulk plume so that the new scheme can contain two plumes at a given time and location: one for shallow and one for deep convection. The mixing characteristic (i.e., inhomogeneous mixing and buoyancy-sorting determination of the entrainment and detrainment rate) of the two plumes is identical to the original plume described in Bretherton et al. (2004), except the fractional lateral mixing rate of a plume ε is parameterized differently. In Bretherton et al. (2004), ε is formulated to be constant with height and inversely proportional to the depth of cumulus top H (i.e., $\varepsilon = c_0/H$; here, c_0 is a nondimensional adjustable parameter). The scaling of ε by H allows a plume to penetrate deeper in deep convective regions, offering a possibility for a single plume to represent both shallow and deep convection (Zhao et al. 2009; Z14). Since we separate explicitly the representation of shallow and deep plumes in the double plume scheme, we adopt a formulation of shallow plume ε_s that decreases with height z as the plume ascends (i.e., $\varepsilon_s = c_0/z$). The scaling of ε_s with height z is supported by results of large-eddy simulations of shallow cumulus convection (e.g., de Roode and Duynkerke 2000; Siebesma et al. 2007).

In addition, the fractional lateral mixing rate of the deep plume ε_d is parameterized to be a linear function

of column relative humidity (CRH is vertically integrated specific humidity divided by vertically integrated saturation specific humidity):

$$\varepsilon_d = \varepsilon_1 + \frac{\mathrm{CRH} - \mathrm{CRH}_0}{1 - \mathrm{CRH}_0}(\varepsilon_2 - \varepsilon_1), \quad \text{for}$$
$$\mathrm{CRH}_0 \le \mathrm{CRH} \le 1, \tag{A1}$$

where $\mathrm{CRH}_0 = 0.5$, $\varepsilon_1 = 1.5 \times 10^{-3}\,\mathrm{m}^{-1}$, and $\varepsilon_2 = 0.5 \times 10^{-4}\,\mathrm{m}^{-1}$. Deep plumes occur only when ambient CRH exceeds CRH_0. Reducing the lateral mixing rate in a more humid environment attempts to roughly account for the effect of convective organization on cumulus entrainment. An introduction of relative humidity–dependent entrainment rate has previously been shown to improve model simulations of MJO and other tropical variability and is generally supported by observational and modeling studies (e.g., Bechtold et al. 2008).

We use a convective available potential energy (CAPE) relaxation closure to determine the cloud-base mass flux for the deep plume (e.g., Zhang and McFarlane 1995; Bechtold et al. 2008). The shallow convective closure was described in Bretherton et al. (2004) and is not changed. The CAPE relaxation time scale for deep convection is 8 h. As discussed in section 2, we have implemented three different options for removing convective precipitation, which apply to both shallow and deep plumes. The model cloud feedback sensitivity to the treatment of the convective precipitation is the key for this study. Convective precipitation is allowed to reevaporate when falling through a subsaturated environment similar to that used in the relaxed Arakawa–Schubert scheme in AM2 (Anderson et al. 2004). The modifications do not include an explicit representation of convective downdrafts, but the precipitation reevaporation in deep plumes appears to be able to produce a sufficient cold pool effect.

We find the above modifications help to substantially reduce model biases in simulating the equatorial eastern Pacific sea surface temperatures, precipitation response to ENSO, and the MJO. The causes for these improvements are currently under investigation and will be reported in upcoming papers.

REFERENCES

Anderson, J. L., and Coauthors, 2004: The new GFDL global atmosphere and land model AM2–LM2: Evaluation with prescribed SST simulations. *J. Climate*, **17**, 4641–4673, doi:10.1175/JCLI-3223.1.

Arakawa, A., and W. H. Schubert, 1974: Interaction of a cumulus cloud ensemble with the large-scale environment, part I. *J. Atmos. Sci.*, **31**, 674–701, doi:10.1175/1520-0469(1974)031<0674:IOACCE>2.0.CO;2.

Bechtold, P., M. Kohler, T. Jung, F. Doblas-Reyes, M. Leutbecher, M. Rodwell, F. Vitart, and G. Balsamo, 2008: Advances in simulating atmospheric variability with the ECMWF model: From synoptic to decadal time-scales. *Quart. J. Roy. Meteor. Soc.*, **134**, 1337–1351, doi:10.1002/qj.289.

Betts, A. K., and Harshvardhan, 1987: Thermodynamic constraint on the cloud liquid water feedback in climate models. *J. Geophys. Res.*, **92**, 8483–8485, doi:10.1029/JD092iD07p08483.

Bony, S., and J.-L. Dufresne, 2005: Marine boundary layer clouds at the heart of tropical cloud feedback uncertainties in climate models. *Geophys. Res. Lett.*, **32**, L20806, doi:10.1029/2005GL023851.

——, ——, H. L. Treut, J.-J. Morcrette, and C. Senior, 2004: On dynamic and thermodynamic components of cloud changes. *Climate Dyn.*, **22**, 71–86, doi:10.1007/s00382-003-0369-6.

——, and Coauthors, 2006: How well do we understand and evaluate climate change feedback processes? *J. Climate*, **19**, 3445–3482, doi:10.1175/JCLI3819.1.

——, and Coauthors, 2015: Clouds, circulation and climate sensitivity. *Nat. Geosci.*, **8**, 261–268, doi:10.1038/ngeo2398.

Bretherton, C. S., 2015: Insights into low-latitude cloud feedbacks from high-resolution models. *Philos. Trans. Roy. Soc. London*, **A373**, 20140415, doi:10.1098/rsta.2014.0415.

——, J. R. McCaa, and H. Grenier, 2004: A new parameterization for shallow cumulus convection and its application to marine subtropical cloud-topped boundary layers. Part I: Description and 1D results. *Mon. Wea. Rev.*, **132**, 864–882, doi:10.1175/1520-0493(2004)132<0864:ANPFSC>2.0.CO;2.

——, P. N. Blossey, and M. Khairoutdinov, 2005: An energy-balance analysis of deep convective self-aggregation above uniform SST. *J. Atmos. Sci.*, **62**, 4273–4292, doi:10.1175/JAS3614.1.

——, ——, and C. Jones, 2013: Mechanisms of marine low cloud sensitivity to idealized climate perturbations: A single-LES exploration extending the CGILS cases. *J. Adv. Model. Earth Syst.*, **5**, 316–337, doi:10.1002/jame.20019.

——, ——, and C. Stan, 2014: Cloud feedbacks on greenhouse warming in the superparameterized climate model SP-CCSM4. *J. Adv. Model. Earth Syst.*, **6**, 1185–1204, doi:10.1002/2014MS000355.

Brient, F., and S. Bony, 2012: How may low-cloud radiative properties simulated in the current climate influence low-cloud feedbacks under global warming? *Geophys. Res. Lett.*, **39**, L20807, doi:10.1029/2012GL053265.

——, and ——, 2013: Interpretation of the positive low-cloud feedback predicted by a climate model under global warming. *Climate Dyn.*, **40**, 2415–2431, doi:10.1007/s00382-011-1279-7.

——, T. Schneider, Z. Tan, and S. Bony, 2015: Shallowness of tropical low clouds as a predictor of climate models' response to warming. *Climate Dyn.*, doi:10.1007/s00382-015-2846-0.

Cess, R., and Coauthors, 1990: Intercomparison and interpretation of climate feedback processes in 19 atmospheric general circulation models. *J. Geophys. Res.*, **95**, 16 601–16 615, doi:10.1029/JD095iD10p16601.

——, and Coauthors, 1996: Cloud feedback in atmospheric general circulation model: An update. *J. Geophys. Res.*, **101**, 12 791–12 794, doi:10.1029/96JD00822.

de Roode, S., and P. Duynkerke, 2000: Analogies between mass-flux and Reynolds-averaged equations. *J. Atmos. Sci.*, **57**, 1585–1598, doi:10.1175/1520-0469(2000)057<1585:ABMFAR>2.0.CO;2.

Donner, L. J., and Coauthors, 2011: The dynamical core, physical parameterizations, and basic simulation characteristics of the atmospheric component AM3 of the GFDL global

coupled model CM3. *J. Climate*, **24**, 3484–3519, doi:10.1175/2011JCLI3955.1.

Donohoe, A., K. C. Armour, A. G. Pendergrass, and D. S. Battisti, 2014: Shortwave and longwave radiative contributions to global warming under increasing CO_2. *Proc. Natl. Acad. Sci. USA*, **111**, 16 700–16 705, doi:10.1073/pnas.1412190111.

Dufresne, J.-L., and S. Bony, 2008: An assessment of the primary sources of spread of global warming estimates from coupled atmosphere–ocean models. *J. Climate*, **21**, 5135–5144, doi:10.1175/2008JCLI2239.1.

Emanuel, K. A., 1991: A scheme for representing cumulus convection in large-scale models. *J. Atmos. Sci.*, **48**, 2313–2335, doi:10.1175/1520-0469(1991)048<2313:ASFRCC>2.0.CO;2.

——, and M. Zivkovic-Rothman, 1999: Development and evaluation of a convection scheme for use in climate models. *J. Atmos. Sci.*, **56**, 1766–1782, doi:10.1175/1520-0469(1999)056<1766:DAEOAC>2.0.CO;2.

——, A. Wing, and E. Vincent, 2013: Radiative-convective instability. *J. Adv. Model. Earth Syst.*, **6**, 75–90, doi:10.1002/2013MS000270.

Flato, G., and Coauthors, 2013: Evaluation of climate models. *Climate Change 2013: The Physical Science Basis*, T. F. Stocker et al., Eds., Cambridge University Press, 741–866. [Available online at https://www.ipcc.ch/pdf/assessment-report/ar5/wg1/WG1AR5_Chapter09_FINAL.pdf.]

Golaz, J.-C., L. Horowitz, and H. Levy II, 2013: Cloud tuning in a coupled climate model: Impact on 20th century warming. *Geophys. Res. Lett.*, **40**, 2246–2251, doi:10.1002/grl.50232.

Gregory, D., and P. R. Rowntree, 1990: A mass flux scheme with representation of cloud ensemble characteristics and stability-dependent closure. *Mon. Wea. Rev.*, **118**, 1483–1506, doi:10.1175/1520-0493(1990)118<1483:AMFCSW>2.0.CO;2.

Hartmann, D., and K. Larson, 2002: An important constraint on tropical cloud–climate feedback. *Geophys. Res. Lett.*, **29**, 1951, doi:10.1029/2002GL015835.

Held, I. M., and B. J. Soden, 2006: Robust responses of the hydrological cycle to global warming. *J. Climate*, **19**, 5686–5699, doi:10.1175/JCLI3990.1.

——, M. Zhao, and B. Wyman, 2007: Dynamic radiative–convective equilibria using GCM column physics. *J. Atmos. Sci.*, **64**, 228–238, doi:10.1175/JAS3825.11.

Joshi, M. M., M. J. Webb, A. C. Maycock, and M. Collins, 2010: Stratospheric water vapour and high climate sensitivity in a version of the HadSM3 climate model. *Atmos. Chem. Phys.*, **10**, 7161–7167, doi:10.5194/acp-10-7161-2010.

Lindzen, R., M.-D. Chou, and A. Hou, 2001: Does the earth have an adaptive infrared iris. *Bull. Amer. Meteor. Soc.*, **82**, 417–432, doi:10.1175/1520-0477(2001)082<0417:DTEHAA>2.3.CO;2.

Mauritsen, T., and B. Stevens, 2015: Missing iris effect as a possible cause of muted hydrological change and high climate sensitivity in models. *Nat. Geosci.*, **8**, 346–351, doi:10.1038/ngeo2414.

Medeiros, B., B. Stevens, I. Held, M. Zhao, D. Williamson, J. Olson, and C. Bretherton, 2008: Aquaplanets, climate sensitivity, and low clouds. *J. Climate*, **21**, 4974–4991, doi:10.1175/2008JCLI1995.1.

Mitchell, J., C. Senior, and W. Ingram, 1989: CO_2 and climate: A missing feedback? *Nature*, **341**, 132–134, doi:10.1038/341132a0.

Moorthi, S., and M. Suarez, 1992: Relaxed Arakawa Schubert: A parameterization of moist convection for general circulation models. *Mon. Wea. Rev.*, **120**, 978–1002, doi:10.1175/1520-0493(1992)120<0978:RASAPO>2.0.CO;2.

Muller, C., and I. Held, 2012: Detailed investigation of the self-aggregation of convection in cloud-resolving simulations. *J. Atmos. Sci.*, **69**, 2551–2565, doi:10.1175/JAS-D-11-0257.1.

Murphy, J. M., D. M. H. Sexton, D. N. Barnett, G. S. Jones, M. J. Webb, M. Collins, and D. A. Stainforth, 2004: Quantification of modelling uncertainties in a large ensemble of climate change simulations. *Nature*, **430**, 768–772, doi:10.1038/nature02771.

Nuijens, L., B. Stevens, and A. Siebesma, 2009: The environment of precipitating shallow cumulus convection. *J. Atmos. Sci.*, **66**, 1962–1979, doi:10.1175/2008JAS2841.1.

Randall, D., and Coauthors, 2007: Climate models and their evaluation. *Climate Change 2007: The Physical Science Basis*, S. Solomon et al., Eds., Cambridge University Press, 589–662. [Available online at https://www.ipcc.ch/pdf/assessment-report/ar4/wg1/ar4-wg1-chapter8.pdf.]

Rayner, R., D. Parker, E. Horton, C. Folland, L. Alexander, and D. Rowel, 2003: Global analyses of sea surface temperature, sea ice, and night marine air temperature since the late nineteenth century. *J. Geophys. Res.*, **108**, 4407, doi:10.1029/2002JD002670.

Rieck, M., L. Nuijens, and B. Stevens, 2012: Marine boundary layer cloud feedbacks in a constant relative humidity atmosphere. *J. Atmos. Sci.*, **69**, 2538–2550, doi:10.1175/JAS-D-11-0203.1.

Ringer, M., and Coauthors., 2006: Global mean cloud feedbacks in idealized climate change experiments. *Geophys. Res. Lett.*, **33**, L07718, doi:10.1029/2005GL025370.

——, T. Andrews, and M. Webb, 2014: Global-mean radiative feedbacks and forcing in atmosphere-only and coupled atmosphere–ocean climate change experiments. *Geophys. Res. Lett.*, **41**, 4035–4042, doi:10.1002/2014GL060347.

Roeckner, E., U. Schlese, J. Biercamp, and P. Loewe, 1987: Cloud optical depth feedbacks and climate modelling. *Nature*, **329**, 138–140, doi:10.1038/329138a0.

Sanderson, B. M., C. Piani, W. J. Ingram, D. A. Stone, and M. R. Allen, 2008: Towards constraining climate sensitivity by linear analysis of feedback patterns in thousands of perturbed-physics GCM simulations. *Climate Dyn.*, **30**, 175–190, doi:10.1007/s00382-007-0280-7.

——, K. M. Shell, and W. Ingram, 2010: Climate feedbacks determined using radiative kernels in a multi-thousand member ensemble of AOGCMs. *Climate Dyn.*, **35**, 1219–1236, doi:10.1007/s00382-009-0661-1.

Senior, C. A., and J. F. B. Mitchell, 1993: Carbon dioxide and climate: The impact of cloud parameterization. *J. Climate*, **6**, 393–418, doi:10.1175/1520-0442(1993)006<0393:CDACTI>2.0.CO;2.

Sherwood, S., S. Bony, and J.-L. Dufresne, 2014: Spread in model climate sensitivity traced to atmospheric convective mixing. *Nature*, **505**, 37–42, doi:10.1038/nature12829.

Siebesma, A., P. Soares, and J. Teixeira, 2007: A combined eddy-diffusivity mass-flux approach for the convective boundary layer. *J. Atmos. Sci.*, **64**, 1230–1248, doi:10.1175/JAS3888.1.

Smith, G. L., K. J. Priestley, N. G. Loeb, B. A. Wielicki, T. P. Charlock, P. Minnis, D. R. Doelling, and D. A. Rutan, 2011: Clouds and Earth Radiant Energy System (CERES), a review: Past, present and future. *Adv. Space Res.*, **48**, 254–263, doi:10.1016/j.asr.2011.03.009.

Soden, B., and I. Held, 2006: An assessment of climate feedbacks in coupled ocean–atmosphere models. *J. Climate*, **19**, 3354–3360, doi:10.1175/JCLI3799.1.

——, A. Broccoli, and R. Hemler, 2004: On the use of cloud forcing to estimate cloud feedback. *J. Climate*, **17**, 3661–3665, doi:10.1175/1520-0442(2004)017<3661:OTUOCF>2.0.CO;2.

——, I. Held, R. Colman, K. Shell, J. Kiehl, and C. Shields, 2008: Quantifying climate feedbacks using radiative kernels. *J. Climate*, **21**, 3504–3520, doi:10.1175/2007JCLI2110.1.

Somerville, R., and L. A. Remer, 1984: Cloud optical thickness feedbacks in the CO_2 climate problem. *J. Geophys. Res.*, **89**, 9668–9672, doi:10.1029/JD089iD06p09668.

Song, X., and G. J. Zhang, 2011: Microphysics parameterization for convective clouds in a global climate model: Description and single-column model test. *J. Geophys. Res.*, **116**, D02201, doi:10.1029/2010JD014833.

Stainforth, D. A., and Coauthors, 2005: Uncertainty in predictions of the climate response to rising levels of greenhouse gases. *Nature*, **433**, 403–406, doi:10.1038/nature03301.

Stephens, G., 2005: Cloud feedbacks in the climate system: A critical review. *J. Climate*, **18**, 237–273, doi:10.1175/JCLI-3243.1.

——, and T. D. Ellis, 2008: Controls of global-mean precipitation increases in global warming GCM experiments. *J. Climate*, **21**, 6141–6155, doi:10.1175/2008JCLI2144.1.

——, and Coauthors, 2010: Dreary state of precipitation in global models. *J. Geophys. Res.*, **115**, D24211, doi:10.1029/2010JD014532.

Stevens, B., and S. Bony, 2013: What are climate models missing? *Science*, **340**, 1053–1054, doi:10.1126/science.1237554.

——, and Coauthors, 2013: The atmospheric component of the MPI-M earth system model: ECHAM6. *J. Adv. Model. Earth Syst.*, **5**, 146–172, doi:10.1002/jame.20015.

Suzuki, K., J.-C. Golaz, and G. Stephens, 2013: Evaluating cloud tuning in a climate model with satellite observations. *Geophys. Res. Lett.*, **40**, 4464–4468, doi:10.1002/grl.50874.

Tiedtke, M., 1989: A comprehensive mass flux scheme for cumulus parameterization in large-scale models. *Mon. Wea. Rev.*, **117**, 1779–1800, doi:10.1175/1520-0493(1989)117<1779:ACMFSF>2.0.CO;2.

Tobin, I., S. Bony, and R. Roca, 2012: Observational evidence for relationships between the degree of aggregation of deep convection, water vapor, surface fluxes, and radiation. *J. Climate*, **25**, 6885–6904, doi:10.1175/JCLI-D-11-00258.1.

Vial, J., J.-L. Dufresne, and S. Bony, 2013: On the interpretation of inter-model spread in CMIP5 climate sensitivity estimates. *Climate Dyn.*, **41**, 3339–3362, doi:10.1007/s00382-013-1725-9.

Walsh, K., and Coauthors, 2015: Hurricanes and climate: The U.S. CLIVAR Working Group on Hurricanes. *Bull. Amer. Meteor. Soc.*, **96**, 997–1017, doi:10.1175/BAMS-D-13-00242.1.

Webb, M., and Coauthors, 2006: On the contribution of local feedback mechanisms to the range of climate sensitivity in two GCM ensembles. *Climate Dyn.*, **27**, 17–38, doi:10.1007/s00382-006-0111-2.

——, F. H. Lambert, and J. Gregory, 2013: Origins of differences in climate sensitivity, forcing and feedback in climate models. *Climate Dyn.*, **40**, 677–707, doi:10.1007/s00382-012-1336-x.

——, and Coauthors, 2015: The impact of parametrized convection on cloud feedback. *Philos. Trans. Roy. Soc. London*, **A373**, 20140414, doi:10.1098/rsta.2014.0414.

Wetherald, R. T., and S. Manabe, 1988: Cloud feedback processes in a general circulation model. *J. Atmos. Sci.*, **45**, 1397–1415, doi:10.1175/1520-0469(1988)045<1397:CFPIAG>2.0.CO;2.

Wyant, M. C., C. S. Bretherton, J. T. Bacmeister, J. T. Kiehl, I. M. Held, M. Zhao, S. A. Klein, and B. J. Soden, 2006: A comparison of low-latitude cloud properties and their response to climate change in three AGCMs sorted into regimes using mid-tropospheric vertical velocity. *Climate Dyn.*, **27**, 261–279, doi:10.1007/s00382-006-0138-4.

——, ——, and P. Blossey, 2009: Subtropical low cloud response to a warmer climate in a superparameterized climate model. Part I: Regime sorting and physical mechanisms. *J. Adv. Model. Earth Syst.*, **1**, 7, doi:10.3894/JAMES.2009.1.7.

Zelinka, M., K. Klein, K. Taylor, T. Andrews, M. Webb, J. Gregory, and P. Forster, 2013: Contributions of different cloud types to feedbacks and rapid adjustments in CMIP5. *J. Climate*, **26**, 5007–5027, doi:10.1175/JCLI-D-12-00555.1.

Zhang, G. J., and N. A. McFarlane, 1995: Sensitivity of climate simulations to the parameterization of cumulus convection in the Canadian climate centre general circulation model. *Atmos.–Ocean*, **33**, 407–446, doi:10.1080/07055900.1995.9649539.

Zhang, M., J. Hack, J. Kiehl, and R. Cess, 1994: Diagnostic study of climate feedback processes in atmospheric general circulation models. *J. Geophys. Res.*, **99**, 5525–5537, doi:10.1029/93JD03523.

——, and Coauthors, 2013: CGILS: Results from the first phase of an international project to understand the physical mechanisms of low cloud feedbacks in single column models. *J. Adv. Model. Earth Syst.*, **5**, 826–842, doi:10.1002/2013MS000246.

Zhao, M., 2014: An investigation of the connections among convection, clouds, and climate sensitivity in a global climate model. *J. Climate*, **27**, 1845–1862, doi:10.1175/JCLI-D-13-00145.1.

——, I. M. Held, S.-J. Lin, and G. A. Vecchi, 2009: Simulations of global hurricane climatology, interannual variability, and response to global warming using a 50-km resolution GCM. *J. Climate*, **22**, 6653–6678, doi:10.1175/2009JCLI3049.1.